Evolution of the spectral weight in the Mott-Hubbard series $SrVO_3$-$CaVO_3$-$LaVO_3$-YVO_3

R. J. O. Mossanek,[1] M. Abbate,[1] T. Yoshida,[2] A. Fujimori,[2] Y. Yoshida,[3] N. Shirakawa,[3] H. Eisaki,[3] S. Kohno,[4] and F. C. Vicentin[5]

[1]*Departamento de Física, Universidade Federal do Paraná, Caixa Postal 19081, 81531-990 Curitiba PR, Brazil*

[2]*Department of Complexity Science and Engineering, University of Tokyo, Kashiwa, Chiba 277-856, Japan*

[3]*Nanoelectronics Research Institute, AIST, 1-1-1 Central 2, Umezono, Tsukuba, Ibaraki, 305-8568, Japan*

[4]*Department of Applied Electronics, Tokyo University of Science, Noda, Chiba 278-8510, Japan*

[5]*Laboratório Nacional de Luz Síncrotron, Caixa Postal 6192, 13083-970 Campinas SP, Brazil*

(Received 7 March 2008; revised manuscript received 15 May 2008; published 5 August 2008)

We studied the Mott-Hubbard series $SrVO_3$-$CaVO_3$-$LaVO_3$-YVO_3 with high-energy photoemission. The features in the experimental spectra were interpreted using cluster model calculations. The valence-band photoemission results show very interesting trends across the Mott-Hubbard series: (i) From $SrVO_3$ to $CaVO_3$, the spectral weight is transferred from the *coherent* to the *incoheren*t feature. (ii) From $CaVO_3$ to $LaVO_3$, the coherent structure disappears, opening the insulating band gap. (iii) Finally, from $LaVO_3$ to YVO_3, the bandwidth of the remaining incoherent feature further decreases. There is also a considerable V 3*d* spectral weight contribution mixed in the O 2*p* band region in all cases. These results suggest that the O 2*p* states play an important role in the Mott-Hubbard transition. Some of the changes in the spectra are unexpected and cannot be explained by the current Mott-Hubbard theories. The calculation reproduces not only the coherent and incoherent structures in the V 3*d* band but also the main features in the O 2*p* band. In addition, the same model explains the charge-transfer satellites observed in the V 2*p* core-level spectra.

DOI: 10.1103/PhysRevB.78.075103 PACS number(s): 71.28.+d, 71.30.+h, 79.60.Bm

I. INTRODUCTION

Substitution induces very interesting changes in the electrical and magnetic properties of transition-metal oxides. For example, it produces the high-T_C superconductivity in $La_{2-x}Sr_xCuO_4$ and the colossal magnetoresistance in $La_{1-x}Sr_xMnO_3$. Substitution also generates Mott-Hubbard transitions in early transition-metal oxides such as $La_{1-x}Sr_xVO_3$. These metal-insulator transitions (MIT) are usually classified according to the main controlling mechanism.[1] In the bandwidth control, the substitution induces a lattice distortion and thus changes in the 3*d* dispersion. In the band-filling control, the doping produces changes in the chemical potential and thus in the 3*d* occupation.

One of the main experimental techniques used to study these transitions is photoemission spectroscopy (PES). The V 3*d* band of $SrVO_3$ showed a *coherent* peak at the Fermi level and a broader *incoherent* structure at higher binding energies.[2,3] Recent works suggested that the differences in the surface vs bulk correlation might affect the PES spectra.[4,5] This prompted the development of hard x-ray photoemission (HXPES) because the larger probing depth would enhance the bulk contribution. This technique was applied to high-T_C superconductivity in $La_{2-x}Sr_xCuO_4$,[6] colossal magnetoresistance in $La_{1-x}Sr_xMnO_3$,[7] and temperature induced MIT in V_2O_3 (Refs. 8 and 9) and VO_2.[10]

The bandwidth controlled MIT in $Sr_{1-x}Ca_xVO_3$ was studied using low-energy (up to 60 eV),[11,12] medium-energy (up to 900 eV),[13] and high-energy (up to 1486 eV)[14] photoemissions. The band-filling controlled MIT in $Y_{1-x}Ca_xVO_3$ was studied using low-energy (up to 60 eV)[15] photoemission, whereas the MIT in $La_{1-x}Ca_xVO_3$ was investigated with high-energy (up to 1486 eV)[16,17] photoemission. Most of these studies were performed at low energy and were mainly concerned with the V 3*d* band. In addition, the comparison with theory in most of these studies was also focused on the V 3*d* region. The $Sr_{1-x}Ca_xVO_3$ (Ref. 14) and the $La_{1-x}Ca_xVO_3$ (Ref. 17) materials were also studied using the V 2*p* core-level photoemission. But the important charge-transfer satellites in the spectra were neither presented nor discussed.

In this work, we study the electronic structure of the Mott-Hubbard series $SrVO_3$-$CaVO_3$-$LaVO_3$-YVO_3. These series include both bandwidth and band-filling control, whereas the previous studies were concerned with either bandwidth or band-filling control. The $SrVO_3$ and $CaVO_3$ compounds are paramagnetic metals with a nominal occupation of $3d^1$ (V^{4+}). The differences in the ionic radii cause a decrease in the V-O-V angle from 180° in $SrVO_3$ to 160° in $CaVO_3$. This change affects the V 3*d* dispersion and consequently the effective V 3*d* one-electron bandwidth. The $LaVO_3$ and YVO_3 materials are antiferromagnetic insulators with a nominal valence of $3d^2$ (V^{3+}). The larger band filling inhibits the coherent charge fluctuations and induces a metal-insulator transition. The V-O-V angle decreases from 158° in $LaVO_3$ to 144° in YVO_3 affecting again the one-electron bandwidth.

The electronic structure of these compounds is studied here using a higher-energy (1840 eV) photoemission. The mean probing depth at this energy, about 25 Å, is larger than in most previous studies, around 5–20 Å.[18] The different features in the experimental spectra are analyzed in terms of cluster model calculations. The calculation reproduces not only the coherent and incoherent structures in the V 3*d* band but also the main features in the O 2*p* band. The valence-band photoemission results show very interesting trends across the Mott-Hubbard series. Some of the changes in the spectra are unexpected and cannot be explained by the current Mott-Hubbard theories. In addition, the same model ex-

plains the charge-transfer satellites observed in the V $2p$ core-level spectra.

II. EXPERIMENTAL DETAILS

The $SrVO_3$, $CaVO_3$, $LaVO_3$, and YVO_3 samples were single crystals grown by the floating zone method. The samples presented a single phase structure as confirmed by using powder x-ray diffraction. The photoemission spectra were measured at room temperature at the SXS beamline in the LNLS (Brazil).[19] The beamline has a double-crystal monochromator equipped with a pair of InSb(111) single crystals. The electron energy analyzer was a Perkin-Elmer and the base pressure was in the $(1-2)\times10^{-9}$ mbar range. The photon energy was set to 1840 eV and the combined energy resolution was approximately 0.4 eV. The spectra were normalized to the maximum and the Fermi level was determined using a clean gold foil. The samples were repeatedly scrapped with a diamond file to remove the surface contamination. The surface quality of the samples was confirmed by the absence of a shoulder in the O 1s core-level spectra.

III. CALCULATION DETAILS

The experimental spectra were interpreted in terms of cluster model calculations. The VO_6 cluster was solved within the usual configuration-interaction method.[20,21] In this method, the transition-metal ground state is expanded in the $3d^n$, $3d^{n+1}\underline{L}$, $3d^{n+2}\underline{L}^2$, etc., configurations, where $\underline{L}$ denotes a hole in the O $2p$ band. The main parameters are the charge-transfer energy Δ, the Mott-Hubbard repulsion U, the transfer integral $pd\sigma$, and the core hole potential Q ($Q=1.25U$).[20,21] The multiplet effects were described by the crystal-field splitting 10 Dq, the intra-atomic exchange J, and the p-p transfer integral ($pp\pi$-$pp\sigma$). The removal (core-level) state is obtained by removing a V $3d$ (core-level) electron from the ground state. The V $3d$ part was calculated using the sudden approximation and the O $2p$ part using the single-particle approach.[22]

In addition to the usual screening from the oxygen sites, the calculation included different *nonlocal* screening channels. For metallic $SrVO_3$ and $CaVO_3$, the model included a nonlocal fluctuation from a coherent state at the Fermi level.[23] Thus, the ground-state expansion contained also the $3d^{n+1}\underline{C}$, $3d^{n+2}\underline{C}^2$, $3d^{n+2}\underline{CL}$, etc., configurations, where $\underline{C}$ denotes a hole in the coherent band. For insulating $LaVO_3$ and YVO_3, the model included a nonlocal Mott-Hubbard fluctuation from a neighboring V ion.[24] Thus, the ground-state expansion contained also the $3d^{n+1}\underline{D}$, $3d^{n+2}\underline{D}^2$, $3d^{n+2}\underline{DL}$, etc., configurations, where $\underline{D}$ denotes a hole in a neighboring V ion. For the metallic (insulating) system, the additional model parameters were the corresponding charge-transfer energy Δ^* (Δ') as well as the effective intercluster transfer integral T^* (T').[25,26] The Δ^* parameter is about half the occupied V $3d$ bandwidth and the Δ' parameter was set equal to the Mott-Hubbard energy U.[25,26] The T' parameter is larger than T^* because there are two $3d$ electrons in the insulating $LaVO_3$ and YVO_3. The parameters used in this work are given in Table I and are the same as obtained for previous lower-energy spectra.[25,26] In addition, these parameters are in good agreement with previous estimates for vanadium oxides.[27,28]

TABLE I. Parameters used in the cluster model calculations (all values in eV).

	$SrVO_3$	$CaVO_3$	$LaVO_3$	YVO_3
Δ	2.0	2.0	3.8	3.8
U	5.0	5.0	4.2	4.2
$pd\sigma$	1.9	1.6	1.8	1.5
10 Dq	1.8	1.5	1.8	1.5
J	0.4	0.4	0.6	0.6
$pp\pi$-$pp\sigma$	0.8	0.8	0.8	0.8
Δ^*	0.75	0.55	-	-
T^*	0.27	0.22	-	-
Δ'	-	-	4.2	4.2
T'	-	-	0.42	0.36

IV. RESULTS AND DISCUSSION

A. Core-level spectra

Figure 1 shows the O 1s and V $2p$ core-level spectra of the $SrVO_3$, $CaVO_3$, $LaVO_3$, and YVO_3 series. The V $2p$

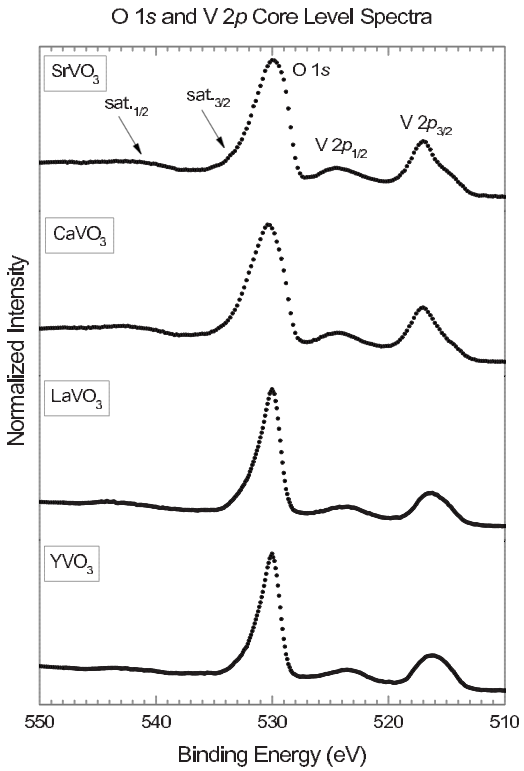

FIG. 1. O 1s and V $2p$ core-level spectra of $SrVO_3$, $CaVO_3$, $LaVO_3$, and YVO_3. The V $2p$ levels are split into the V $2p_{3/2}$ and V $2p_{1/2}$ sublevels. The spectra present charge-transfer satellites associated with each sublevel.

spectrum is split by spin-orbit interactions in the V $2p_{3/2}$ (about 516 eV) and V $2p_{1/2}$ (around 524 eV) regions. The O 1*s* peak (around 530 eV) presents an asymmetric shape in the metallic compounds ($SrVO_3$ and $CaVO_3$) and a narrower and more symmetric profile in the insulating compounds ($LaVO_3$ and YVO_3). This change in the O 1*s* peak, from an asymmetric to a symmetric profile, signals the metal-insulator transition. The same behavior was observed in the O 1*s* spectra of V_2O_3 and VO_2 obtained across the metal-insulator transition.[8,10] The absence of a high-energy shoulder in the O 1*s* spectra confirms the surface quality of the samples.

The V 2*p* part of the core-level spectra also presents relevant changes across the metal-insulator transition. The changes are similar to those observed in the V 2*p* spectra of V_2O_3 and VO_2 across the metal-insulator transition.[8,10] The V $2p_{3/2}$ region in the metallic spectra shows a main peak (around 517 eV) and a shoulder (about 515 eV). The shoulder disappears in the insulating spectra and the main peak shifts to lower energies (around 516 eV). The shift is attributed to a change in the electrostatic environment of the V ions, from a V^{4+} state in the metallic compounds to a V^{3+} state in the insulating materials. Finally, each of the V 2*p* regions presents an associated charge-transfer satellite at higher energies. The satellite corresponding to the V $2p_{3/2}$ level is hidden in the high-energy side of the O 1*s* peak, whereas the satellite associated with the V $2p_{1/2}$ level appears around 542 eV.

Figure 2 presents the calculated core-level spectra of the $SrVO_3$, $CaVO_3$, $LaVO_3$, and YVO_3 series. The labels in the figure indicate the character of the dominant configuration in each of the final states. The transitions were convoluted with a 1.1 eV Gaussian to account for the resolution as well as additional broadening effects, which are not included in the present calculation (V 2*p*-3*d* multiplet splitting, Coster-Kronig transitions, and electron-hole pair creation). Further, the energy scale was adjusted to the binding energy of the corresponding V 2*p* core levels. The O 1*s* peak was simulated using an asymmetric Doniach-Sunjic function for the metallic compounds and a symmetric Lorentzian for the insulating materials. The resulting spectra (full line) are the sum of the calculated spectrum (dashed) and the integrated background (dotted). We describe the calculated spectra of the V $2p_{3/2}$ region and the corresponding charge-transfer satellite. The same description applies to the V $2p_{1/2}$ region and its satellite, which is localized around 542 eV.

The V $2p_{3/2}$ region corresponds to the *well-screened* final states, whereas the satellite is related to the *poorly screened* final states. The main peak in the metallic materials (about 517 eV) is dominated by the ligand screened $\underline{c}3d^2\underline{L}$ configuration (40%–43%), whereas the shoulder (around 515 eV) is mostly attributed to the coherent screened $\underline{c}3d^2\underline{C}$ configuration (30%–32%). The reduced intensity of the shoulder in $CaVO_3$ is due to the decrease in T^* parameter which, in turn, is related to the increase in the orthorhombic distortion in this material. Finally, the charge-transfer satellite (about 533 eV) is mainly related to the $\underline{c}3d^1$ configuration (28%–31%). The main feature in the insulating materials (about 516 eV) is still due to the $\underline{c}3d^3\underline{L}$ configuration (41%–42%). The shoulder disappears in this case because the coherent screening is replaced by a Mott-Hubbard screening. The corresponding screened feature (around 521 eV) is mostly formed by the $\underline{c}3d^3\underline{D}$ configuration (34%–37%). Finally, the charge-transfer satellite in this case (about 533 eV) is related to the $\underline{c}3d^2$ configuration (38%–42%).

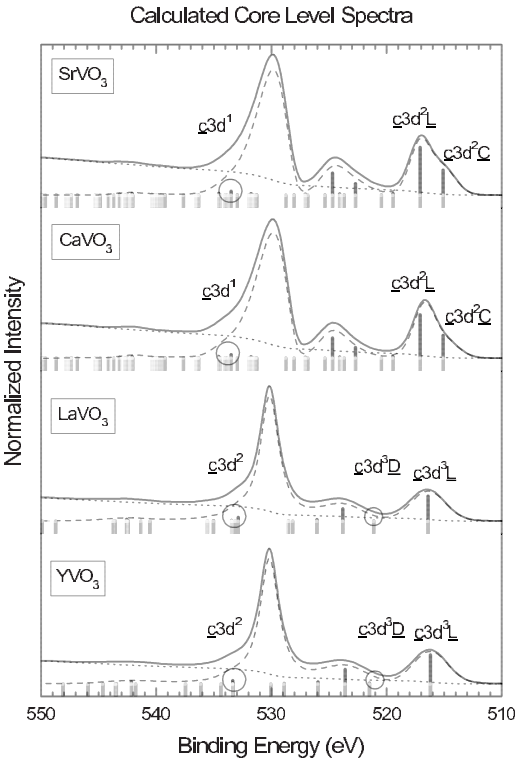

FIG. 2. Calculated core-level spectra of $SrVO_3$, $CaVO_3$, $LaVO_3$, and YVO_3 (solid line). The cluster model calculation (dashed line) is mounted on the background (dotted line). The spectra of $SrVO_3$ and $CaVO_3$ show the *well-screened* ($\underline{c}3d^2\underline{C}$ and $\underline{c}3d^2\underline{L}$) and *poorly screened* ($\underline{c}3d^1$) features, whereas the spectra of $LaVO_3$ and YVO_3 show the well-screened ($\underline{c}3d^3\underline{L}$) and poorly screened ($\underline{c}3d^2$) features.

B. Valence-band spectra

Figure 3 shows the valence-band photoemission spectra of the $SrVO_3$, $CaVO_3$, $LaVO_3$, and YVO_3 series. The vertical bars in the figure indicate the position and evolution of the main structures in the spectra. The spectra are formed by the O 2*p* band from 9.0 to 3.0 eV and the V 3*d* band from 3.0 to 0.0 eV. The V 3*d* region next to the Fermi level was enlarged five times to enhance this relatively weak structure. The O 2*p* band presents a prominent feature around 6.7 eV for $SrVO_3$, which shifts to 6.9 eV for $CaVO_3$, 7.0 eV for $LaVO_3$, and 7.5 eV for YVO_3. The V 3*d* band of metallic $SrVO_3$ and $CaVO_3$ presents two distinct components: the coherent structure around 0.5 eV and the incoherent feature about 1.7 eV. The coherent structure of insulating $LaVO_3$ and YVO_3 is substituted by a feature emerging about 5.1 eV. The disappearance of the coherent structure opens the band gap, whereas the remaining incoherent feature shifts slightly to 1.8 eV. The absence of spurious features around 8–10 eV in the spectra confirms again the quality of the surface.

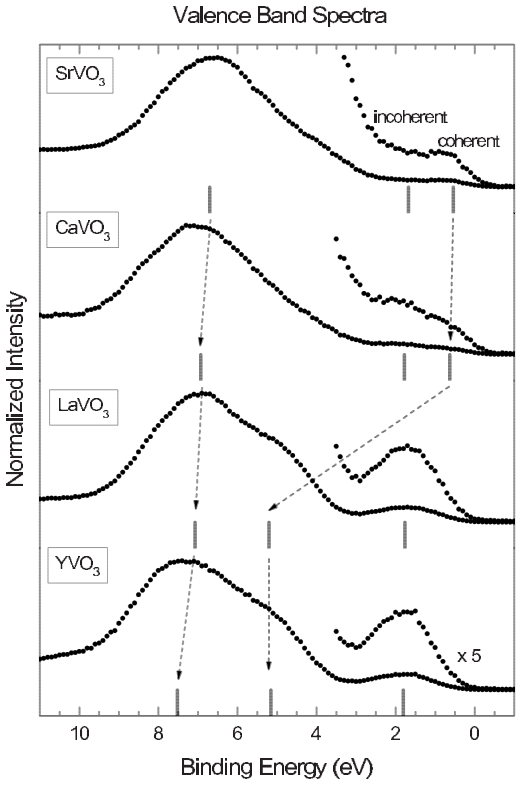

FIG. 3. Valence-band spectra of $SrVO_3$, $CaVO_3$, $LaVO_3$, and YVO_3 taken at 1840 eV. The V 3*d* band region near the Fermi level was augmented five times. The bars indicate the position and evolution of the main structures in the spectra. The V 3*d* band of $SrVO_3$ and $CaVO_3$ shows the *coherent* and *incoherent* features.

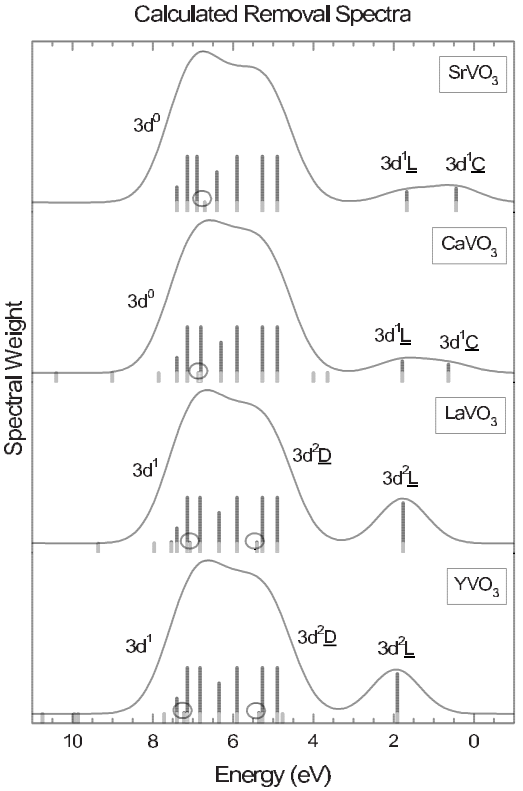

FIG. 4. Calculated removal spectra of $SrVO_3$, $CaVO_3$, $LaVO_3$, and YVO_3. The labels correspond to the main configuration in each final state, see text.

This description of the spectra was motivated and guided by the results of cluster model calculations. Figure 4 shows the calculated valence-band removal spectra of $SrVO_3$, $CaVO_3$, $LaVO_3$, and YVO_3. The transitions were convoluted with a 0.5 eV Gaussian to simulate the band dispersion and the experimental broadening. For the metallic $SrVO_3$ and $CaVO_3$ systems, the calculated V 3*d* band reproduces both the coherent and incoherent peaks. The coherent peak is mainly given by the well-screened final-state $3d^1\underline{C}$ configuration (with 25%–30%) and appears around Δ^*. The incoherent peak is mostly due to the well-screened final-state $3d^1\underline{L}$ configuration (with 35%–40%) and appears around Δ. Finally, there is a weaker V 3*d* removal state contribution mixed in the much more intense O 2*p* band. This structure is related to the poorly screened final-state $3d^0$ configuration (with 50%–55%) and appears at about U.

For insulating $LaVO_3$ and YVO_3, the coherent fluctuation ($3d^2\underline{C}$) is replaced by a Mott-Hubbard screening ($3d^2D$). The transfer of spectral weight from the $3d^2\underline{C}$ to the $3d^2\underline{D}$ final states opens the corresponding band gap. The incoherent peak is mainly due to the well-screened final-state $3d^2\underline{L}$ configuration (with 40%–45%) and appears around Δ. The Mott-Hubbard peak is mostly formed by the final-state $3d^2\underline{D}$ configuration (with 45%–50%) and appears around Δ'. Finally, the poorly screened final-state $3d^1$ configuration contributes mainly to a removal state about U (with 35%–40%).

The calculated V 3*d* removal states above coincide with the main features in the experimental spectra. The dynamical mean-field theory (DMFT) attributes the coherent structure to the quasiparticle peak and the incoherent feature to the remnant of the lower Hubbard band.[4,5] The present cluster model ascribes the coherent feature to the $3d^n\underline{C}$ final state in the same spirit as the quasiparticle peak in DMFT, but the incoherent structure here is attributed to the $3d^n\underline{L}$ configuration. The $3d^{n-1}$ final-state configuration appears mostly mixed with the O 2*p* band at higher energies. Indeed, resonant photoemission experiments in YVO_3 and $CaVO_3$ show considerable V 3*d* character around 7.0 eV (Ref. 15) (although some of these V 3*d* character is also partially due to the covalent hybridization with the O 2*p* states).

The results indicate that $SrVO_3$ and $CaVO_3$ are in the charge-transfer regime because Δ is smaller than U.[29] The ground state of these compounds is highly covalent and is dominated by the $3d^1$ (27%–29%) and $3d^2\underline{L}$ (47%–48%) configurations. However, note that the lowest-energy removal state is dominated by the coherent screened $3d^1\underline{C}$ configuration. On the other hand, $LaVO_3$ and YVO_3 are in a highly mixed intermediate regime because Δ is of the order of U.[29] The ground state of these compounds is less covalent and is dominated by the $3d^2$ (40%–42%) and $3d^3\underline{L}$ (45%–47%) configurations. We note that both the core-level and valence-band spectra can be explained using the same model. Further, a reasonable agreement with the experiment results is obtained using the same parameter set. Thus, the present cluster model provides a consistent description of the electronic structure of these materials.

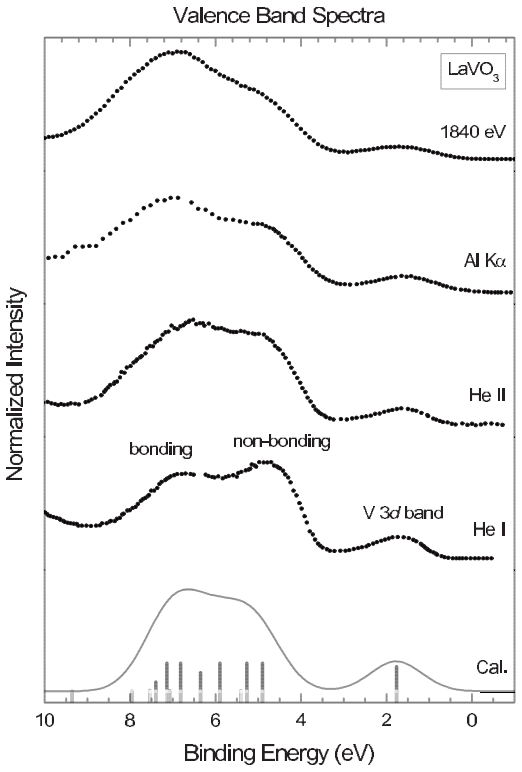

FIG. 5. Valence-band spectra of $LaVO_3$ obtained with different photon energies (the He I, He II, and Al $K\alpha$ spectra were taken from Ref. 17). The spectra can be divided into the bonding O $2p$-V $3d$ band, the nonbonding O $2p$ part, and the V $3d$ region.

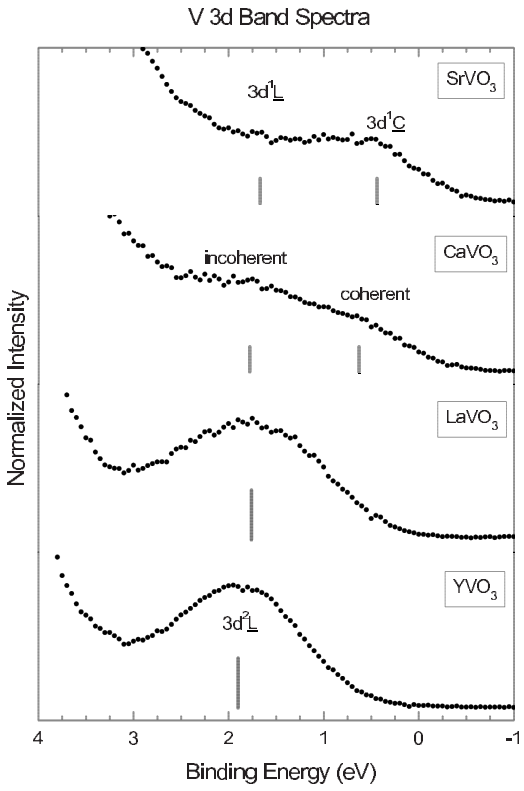

FIG. 6. V $3d$ band spectra of $SrVO_3$, $CaVO_3$, $LaVO_3$, and YVO_3 in more detail. The spectra of $SrVO_3$ and $CaVO_3$ show the coherent ($3d^1\underline{C}$) and incoherent ($3d^1\underline{L}$) features, whereas the spectra of $LaVO_3$ and YVO_3 show only the incoherent ($3d^2\underline{L}$) structure.

C. Photon energy dependence

Figure 5 presents the photoemission spectra of $LaVO_3$ obtained with different photon energies (the He I, He II, and Al $K\alpha$ spectra were taken from Ref. 17). The valence band of this compound can be divided into three main features: a bonding O $2p$-V $3d$ band (from 8.0 to 6.0 eV), an almost pure nonbonding O $2p$ part (from 6.0 to 4.0 eV), and a V $3d$ region (from 3.0 to 0.0 eV). The photoemission spectra exhibit a considerable and continuous variation as a function of the photon energy. In particular, the nonbonding O $2p$ part decreases strongly and the weak V $3d$ band reduces for higher photon energies. In fact, the high-energy photoemission spectrum is dominated by the bonding O $2p$-V $3d$ band, whereas the nonbonding O $2p$ part is strongly suppressed and the V $3d$ region appears diminished. The same spectral shape was observed in the hard x-ray photoemission spectra of the VO_2 compound.[10] These changes in the higher-energy photoemission spectra are surprising and remain unexplained until now.

In a first approximation, it is tempting to relate the changes in the spectra to the photoemission cross section. The calculated spectra resemble the low-energy spectra (He II), where the relative V $3d$/O $2p$ cross section is about 1/1. The relative cross section increases to around 3/2 for high energy (1840 eV), which would explain the decrease in the nonbonding O $2p$ part. But this argument would be at variance with the simultaneous decrease observed in the V $3d$ band region. This discrepancy shows that the differences cannot be attributed entirely to the atomic cross section. The peculiar spectral weight observed in the higher-energy photoemission spectra remains thus elusive. A proper description of the spectra should include a many-body approach to the photoemission process in the solid.

D. V 3*d* band region

Figure 6 presents the V $3d$ band photoemission of $SrVO_3$, $CaVO_3$, $LaVO_3$, and YVO_3 in more detail. The V $3d$ spectral weight follows a very interesting trend as a function of the bandwidth and band-filling control. In metallic $SrVO_3$ and $CaVO_3$, the increased distortion decreases the intercluster transfer T^* and the effective one-electron bandwidth. In turn, the reduction in T^* results in the transfer of spectral weight from the coherent to the incoherent structures. From metallic $CaVO_3$ ($3d^1$) to insulating $LaVO_3$ ($3d^2$), the increased band filling inhibits the coherent charge fluctuations which are responsible for the metallic character. The replacement of the coherent fluctuation ($3d^2\underline{C}$) by the Mott-Hubbard screening ($3d^2\underline{D}$) opens the band gap. Finally, the increase in the orthorhombic distortion in the insulating phase produces an additional effect. The bandwidth of the incoherent feature decreases from around 1.4 eV in $LaVO_3$ to about 1.2 eV in YVO_3.

The local-density approximation cannot reproduce correctly the electronic structure of highly correlated systems. Despite its limitations, this method provides a reasonably

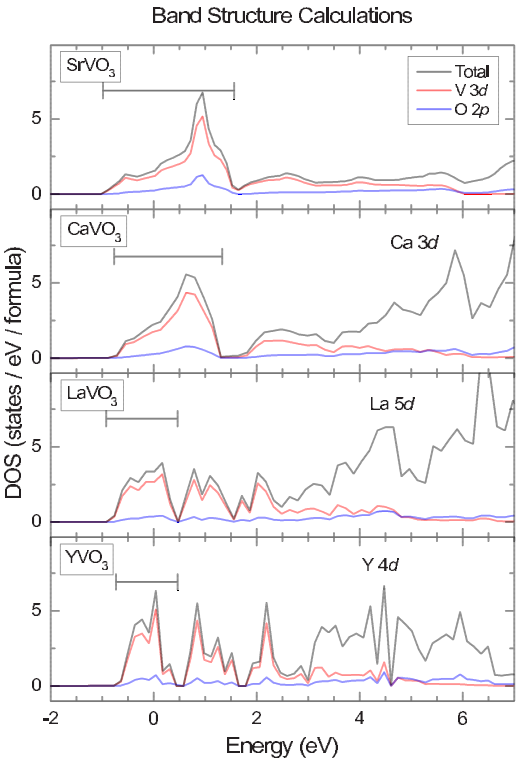

FIG. 7. (Color online) Calculated total and partial densities of states of $SrVO_3$, $CaVO_3$, $LaVO_3$, and YVO_3. The segments indicate the width of the lowest-energy V 3*d* band.

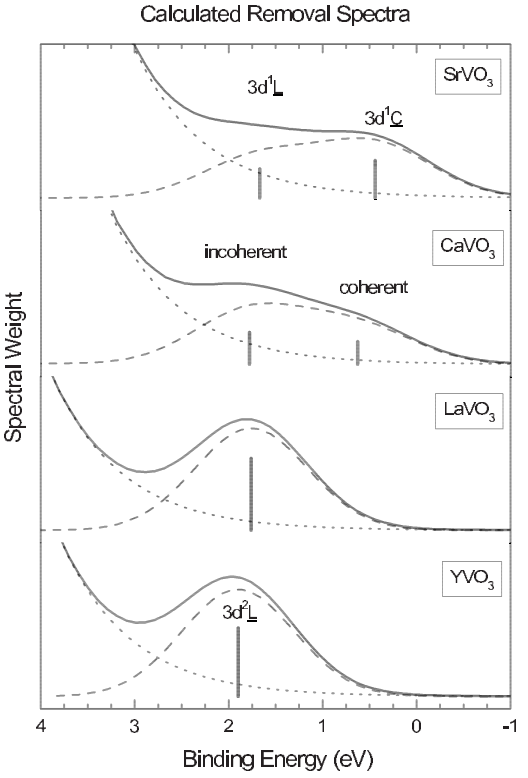

FIG. 8. Calculated removal spectra of $SrVO_3$, $CaVO_3$, $LaVO_3$, and YVO_3 in more detail (solid line). The cluster model calculation (dashed line) is mounted on the background (dotted line). The spectra of $SrVO_3$ and $CaVO_3$ show the coherent ($3d^1C$) and incoherent ($3d^1\underline{L}$) features, whereas the spectra of $LaVO_3$ and YVO_3 show only the incoherent ($3d^2\underline{L}$) structure.

good estimate of the one-electron band dispersion. Figure 7 shows the total and partial densities of states of $SrVO_3$, $CaVO_3$, $LaVO_3$, and YVO_3 in the V 3*d* band region. The calculation was performed with the full-potential linear-muffin-tin-orbital method[30] using the observed crystallographic structure of the different compounds.[31,32] The electronic structure of $SrVO_3$ and $CaVO_3$ was calculated in the paramagnetic phase, whereas the electronic structure of $LaVO_3$ and YVO_3 was calculated in the antiferromagnetic phase. The calculated bandwidth of the lowest-energy V 3*d* band decreases from about 2.7 eV for $SrVO_3$ to 2.0 eV for $CaVO_3$, 1.4 eV for $LaVO_3$, and 1.1 eV for YVO_3 (see Fig. 7). The reduction in the bandwidth can be directly related to the increased orthorhombic distortion in the series, although the band splitting due to the antiferromagnetic ordering also plays a role in $LaVO_3$ and YVO_3. The values for $LaVO_3$ and YVO_3 are strikingly similar to the observed bandwidth of the incoherent structure. The observed changes in the bandwidth of the incoherent feature are not being addressed by the current theories.

Figure 8 presents the calculated V 3*d* removal spectra of $SrVO_3$, $CaVO_3$, $LaVO_3$, and YVO_3 in more detail. The calculated spectrum was mounted on the corresponding background and was convoluted with a Gaussian function. The calculation reproduces the coherent ($3d^1\underline{C}$) and incoherent ($3d^1\underline{L}$) peaks in metallic $SrVO_3$ and $CaVO_3$, as well as the remaining incoherent structure ($3d^2\underline{L}$) in the insulating $LaVO_3$ and YVO_3 compounds. The transfer of spectral weight from the coherent to the incoherent feature—in the metallic systems—is related to the reduction in the V-O-V angle, which decreases the effective T^* hopping. Finally, the band gap in the insulating systems is due to the replacement of the coherent ($3d^2\underline{C}$) by the Mott-Hubbard fluctuation ($3d^2D$).

V. SUMMARY AND CONCLUSION

In conclusion, we studied the Mott-Hubbard series $SrVO_3$-$CaVO_3$-$LaVO_3$-YVO_3 using high-energy spectroscopy. The different features in the experimental spectra were analyzed using cluster model calculations. The V 3*d* removal states present a very interesting trend as a function of bandwidth and band-filling control. (i) The bandwidth control from $SrVO_3$ to $CaVO_3$ transfers spectral weight from the coherent to incoherent feature. (ii) The band filling from $CaVO_3$ to $LaVO_3$ inhibits the coherent charge fluctuations opening the band gap (the coherent structure, in this case, is replaced by a V 3*d* removal state mixed in the O 2*p* band region). (iii) Finally, the bandwidth control from $LaVO_3$ to YVO_3 reduces the width of the remaining incoherent structure. There is also a considerable contribution from V 3*d* removal states mixed in the O 2*p* band region. These results suggest that O 2*p* states play an important role in the Mott-Hubbard transition. Some of these changes are unexpected and cannot be explained by the current Mott-Hubbard theories. The calculation reproduces not only the coherent and

incoherent structures in the V 3*d* band but also the main features in the O 2*p* band. In addition, the same model explains the charge-transfer satellites observed in the V 2*p* core-level spectra.

ACKNOWLEDGMENTS

This work was partially supported by the Brazilian funding agencies CNPq and CAPES.

[1] M. Imada, A. Fujimori, and Y. Tokura, Rev. Mod. Phys. **70**, 1039 (1998).
[2] A. Fujimori, I. Hase, H. Namatame, Y. Fujishima, Y. Tokura, H. Eisaki, S. Uchida, K. Takegahara, and F. M. F. de Groot, Phys. Rev. Lett. **69**, 1796 (1992).
[3] K. Morikawa, T. Mizokawa, K. Kobayashi, A. Fujimori, H. Eisaki, S. Uchida, F. Iga, and Y. Nishihara, Phys. Rev. B **52**, 13711 (1995).
[4] A. Liebsch, Phys. Rev. Lett. **90**, 096401 (2003).
[5] I. A. Nekrasov, G. Keller, D. E. Kondakov, A. V. Kozhevnikov, Th. Pruschke, K. Held, D. Vollhardt, and V. I. Anisimov, Phys. Rev. B **72**, 155106 (2005).
[6] M. Taguchi, A. Chainani, K. Horiba, Y. Takata, M. Yabashi, K. Tamasaku, Y. Nishino, D. Miwa, T. Ishikawa, T. Takeuchi, K. Yamamoto, M. Matsunami, S. Shin, T. Yokoya, E. Ikenaga, K. Kobayashi, T. Mochiku, K. Hirata, J. Hori, K. Ishii, F. Nakamura, and T. Suzuki, Phys. Rev. Lett. **95**, 177002 (2005).
[7] K. Horiba, M. Taguchi, A. Chainani, Y. Takata, E. Ikenaga, D. Miwa, Y. Nishino, K. Tamasaku, M. Awaji, A. Takeuchi, M. Yabashi, H. Namatame, M. Taniguchi, H. Kumigashira, M. Oshima, M. Lippmaa, M. Kawasaki, H. Koinuma, K. Kobayashi, T. Ishikawa, and S. Shin, Phys. Rev. Lett. **93**, 236401 (2004).
[8] N. Kamakura, M. Taguchi, A. Chainani, Y. Takata, K. Horiba, K. Yamamoto, K. Tamasaku, Y. Nishino, D. Miwa, E. Ikenaga, M. Awaji, A. Takeuchi, H. Ohashi, Y. Senba, H. Namatame, M. Taniguchi, T. Ishikawa, K. Kobayashi, and S. Shin, Europhys. Lett. **68**, 557 (2004).
[9] G. Panaccione, M. Altarelli, A. Fondacaro, A. Georges, S. Huotari, P. Lacovig, A. Lichtenstein, P. Metcalf, G. Monaco, F. Offi, L. Paolasini, A. Poteryaev, M. Sacchi, and O. Tjernberg, Phys. Rev. Lett. **97**, 116401 (2006).
[10] R. Eguchi, M. Taguchi, M. Matsunami, K. Horiba, K. Yamamoto, A. Chainani, Y. Takata, M. Yabashi, D. Miwa, Y. Nishino, K. Tamasaku, T. Ishikawa, Y. Senba, H. Ohashi, I. H. Inoue, Y. Muraoka, Z. Hiroi, and S. Shin, J. Electron Spectrosc. Relat. Phenom. **156**, 421 (2007).
[11] I. H. Inoue, I. Hase, Y. Aiura, A. Fujimori, Y. Haruyama, T. Maruyama, and Y. Nishihara, Phys. Rev. Lett. **74**, 2539 (1995).
[12] R. Eguchi, T. Kiss, S. Tsuda, T. Shimojima, T. Mizokami, T. Yokoya, A. Chainani, S. Shin, I. H. Inoue, T. Togashi, S. Watanabe, C. Q. Zhang, C. T. Chen, M. Arita, K. Shimada, H. Namatame, and M. Taniguchi, Phys. Rev. Lett. **96**, 076402 (2006).
[13] A. Sekiyama, H. Fujiwara, S. Imada, S. Suga, H. Eisaki, S. I. Uchida, K. Takegahara, H. Harima, Y. Saitoh, I. A. Nekrasov, G. Keller, D. E. Kondakov, A. V. Kozhevnikov, Th. Pruschke, K. Held, D. Vollhardt, and V. I. Anisimov, Phys. Rev. Lett. **93**, 156402 (2004).
[14] K. Maiti, D. D. Sarma, M. J. Rozenberg, I. H. Inoue, H. Makino, O. Goto, M. Pedio, and R. Cimino, Europhys. Lett. **55**, 246 (2001).
[15] H. F. Pen, M. Abbate, A. Fujimori, Y. Tokura, H. Eisaki, S. Uchida, and G. A. Sawatzky, Phys. Rev. B **59**, 7422 (1999).
[16] K. Maiti, P. Mahadevan, and D. D. Sarma, Phys. Rev. Lett. **80**, 2885 (1998).
[17] K. Maiti and D. D. Sarma, Phys. Rev. B **61**, 2525 (2000).
[18] S. Hüfner, in *Photoelectron Spectroscopy: Principles and Applications*, edited by M. Cardona (Springer-Verlag, Berlin, 1996), p. 8.
[19] M. Abbate, F. C. Vicentin, V. Compagnon-Cailhol, M. C. Rocha, and H. Tolentino, J. Synchrotron Radiat. **6**, 964 (1999).
[20] G. van der Laan, C. Westra, C. Haas, and G. A. Sawatzky, Phys. Rev. B **23**, 4369 (1981).
[21] A. Fujimori and F. Minami, Phys. Rev. B **30**, 957 (1984).
[22] R. J. O. Mossanek and M. Abbate, Phys. Rev. B **74**, 125112 (2006).
[23] A. E. Bocquet, T. Mizokawa, A. Fujimori, M. Matoba, and S. Anzai, Phys. Rev. B **52**, 13838 (1995); M. Taguchi, A. Chainani, N. Kamakura, K. Horiba, Y. Takata, M. Yabashi, K. Tamasaku, Y. Nishino, D. Miwa, T. Ishikawa, S. Shin, E. Ikenaga, T. Yokoya, K. Kobayashi, T. Mochiku, K. Hirata, and K. Motoya, *ibid.* **71**, 155102 (2005).
[24] M. A. van Veenendaal and G. A. Sawatzky, Phys. Rev. Lett. **70**, 2459 (1993); K. Okada and A. Kotani, Phys. Rev. B **52**, 4794 (1995).
[25] R. J. O. Mossanek, M. Abbate, and A. Fujimori, Phys. Rev. B **74**, 155127 (2006).
[26] R. J. O. Mossanek and M. Abbate, Phys. Rev. B **76**, 035101 (2007).
[27] A. E. Bocquet, T. Mizokawa, K. Morikawa, A. Fujimori, S. R. Barman, K. Maiti, D. D. Sarma, Y. Tokura, and M. Onoda, Phys. Rev. B **53**, 1161 (1996).
[28] T. Uozumi, K. Okada, and A. Kotani, J. Phys. Soc. Jpn. **62**, 2595 (1993).
[29] J. Zaanen, G. A. Sawatzky, and J. W. Allen, Phys. Rev. Lett. **55**, 418 (1985).
[30] S. Y. Savrasov, Phys. Rev. B **54**, 16470 (1996).
[31] E. Pavarini, S. Biermann, A. Poteryaev, A. I. Lichtenstein, A. Georges, and O. K. Andersen, Phys. Rev. Lett. **92**, 176403 (2004).
[32] H. Sawada, N. Hamada, K. Terakura, and T. Asada, Phys. Rev. B **53**, 12742 (1996).